SHALLOW FOUNDATION ANALYSIS BY SMOOTHED PARTICLE HYDRODYNAMICS METHOD

V. Emren[1], K. Tuncay[2]

[1]Department of Civil Engineering, ODTU, Ankara, Turkey, vemren@metu.edu.tr
[2]Department of Civil Engineering, ODTU, Ankara, Turkey, tuncay@metu.edu.tr

Abstract

This paper illustrates the use of Smoothed Particle Hydrodynamics (SPH) technique to compute the bearing capacity of shallow foundations and establish their failure mechanism. SPH is a numerical method based on a Lagrangian formulation to solve partial differential equations by discretizing the computational domain with a set of particles that have field variables such as mass, and density. SPH is a meshless method and is not affected by the particles' arbitrariness due to its adaptive nature, and it can naturally handle problems that are caused by large deformations. Non-associated Drucker-Prager model is implemented into the model to simulate the soil behavior. The computed values are then compared with PLAXIS 2D finite element results. Agreements of the results of these two methods show that SPH is potentially a promising method for geotechnical problems experiencing large deformations and mesh distortions.

Keywords: *SPH, FEM, Shallow Foundations*

1 Introduction

Large deformation problems are commonly encountered in geotechnical engineering, and in order to tackle these problems, some numerical methods such as Finite Element Method (FEM), and Discrete Element Method (DEM) are frequently used in the literature. However, FEM has significant disadvantages when it comes to large deformation problems since it undergoes excessive grid-distortion while DEM requires excessive number of particles even for small-scaled problems. Meshless computational methods naturally eliminate the problems that are formerly mentioned. Smoothed Particle Hydrodynamics (SPH) method is one of the meshless computational methods, and it was invented in 1977 in order to model astrophysical problems by Lucy et al. SPH is a Lagrangian meshless method where the computational domain is discretized with a set of particles that have some field variables such as position, velocity, pressure, mass, density etc. Compared with the other mesh-based methods, SPH has several advantages such that since each material type can be modelled in a separate set of particles, there is no interface problem. Furthermore, complex geometries can be handled easily, and large deformation behavior can be captured due to the adaptive nature of SPH. The method can be applied to a wide range of areas from solid mechanics to fluid mechanics. One can find extensive information about SPH from (Monaghan, 1992) and (Monaghan, 2005).

In this study, failure mechanism analysis of shallow foundation penetration into granular soil is discussed. Drucker-Prager model with non-associated flow rule is used to simulate the elasto-plastic behavior of soil, and the SPH results are compared with the PLAXIS 2D finite element solutions, and the failure mechanisms proposed by Terzaghi (1943).

2 Smoothed Particle Hydrodynamics (SPH)

SPH is a method where particle properties change as a function of time and space that is dictated by constitutive and governing partial differential equations.

Interpolated value of a function A at an arbitrary position **x** can be defined using SPH smoothing:

$$A(x) = \sum_{j}^{N} m_j \frac{A(x_j)}{\rho_j} W(|x - x_j|, h)$$

where m_j is the mass, and ρ_j is the density of the neighbor particles, h is the smoothing length, and the summation is done over all particles j within an effective radius. $W(x\text{-}x_j,h)$ is a cubic spline function proposed by Monaghan and Lattanzio (1985) having the following form:

$$W_{ij} = \alpha_d \begin{cases} \frac{2}{3} - q^2 + \frac{1}{2}q^3, & 0 \le q < 1 \\ \frac{1}{6}(2-q)^3, & 1 \le q < 2 \\ 0, & q \ge 2 \end{cases}$$

Where α_d is $15/7\pi h^2$, and q is the normalized distance between the particle of interest and its neighbors that is q = r/h.

The gradient of the function A has the following form:

$$\nabla A(x) = \sum_{j}^{N} \frac{m_j A(x_j)}{\rho_j} \nabla W(x - x_j, h)$$

By incorporating suitable finite difference approximations for second order derivatives with the interpolation formulae given above, it is possible to obtain the required equations to capture the motion of the particles, and rate of change of their properties. These differential equations are presented in the next section.

2.1 Motion Equations

Continuity equation for soil and its SPH discretization are as follows:

$$\frac{d\rho}{dt} = -\rho.\nabla v$$

$$\frac{d\rho_i}{dt} = \sum_{j=1}^{N} m_j (v_i^{\alpha} - v_j^{\alpha}) \frac{\partial W_{ij}}{\partial x_i^{\alpha}}$$

Linear momentum equation and its SPH discretization for all particles as follows:

$$\frac{dv^{\alpha}}{dt} = -\frac{1}{\rho} \frac{\partial \sigma^{\alpha\beta}}{\partial x^{\beta}} + f^{\alpha}$$

$$\frac{dv_i^{\alpha}}{dt} = \sum_{j=1}^{N} m_j \left(\frac{\sigma_i^{\alpha\beta} + \sigma_j^{\alpha\beta}}{\rho_i \rho_j} + C_{ij}^{\alpha\beta} \right) \frac{\partial W_{ij}}{\partial x^{\beta}} + f^{\alpha}$$

where α and β are the Cartesian components x, y with the Einstein convention applied to repeated indices, and i represents the particle of interest, and j represents the neighbor particles, v is the velocity, ρ is the soil density, and $\sigma^{\alpha\beta}$ denotes the total stress tensor for the soil. d/dt represents the material derivative, and f^{α} stands for the external force per unit mass.

$C_{ij}^{\alpha\beta}$ stands for artificial viscosity in order to damp out the unphysical oscillations, and tensile instability (Bui et al., 2008). In this study, in addition to the use of artificial viscosity, a local damping definition is applied to the model. In this approach, out of balance force is calculated, and reduced by 20% for each particle at each time step.

2.2 Soil Constitutive Model

In this study, Drucker – Prager model is used to determine the plastic flow regime of the soil. In this model, yield condition can be expressed as follows:

$$f(I_1, J_2) = \sqrt{J_2} + \alpha_\varphi I_1 - k_c = 0$$

where α_Φ and k_c are the Drucker-Prager's constants while I_1 and J_2 are the first and the second stress tensor invariants, respectively, and they can be expressed as follows:

$$I_1 = \sigma^{xx} + \sigma^{yy} + \sigma^{zz} \quad \& \quad J_2 = \frac{1}{2} s^{\alpha\beta} s^{\alpha\beta}$$

$$\alpha_\varphi = \frac{\tan\varphi}{\sqrt{9 + 12\tan^2\varphi}} \quad \& \quad kc = \frac{3c}{\sqrt{9 + 12\tan^2\varphi}}$$

where $s^{\alpha\beta}$ is the deviatoric shear stress, and $\sigma^{\alpha\alpha}$ is the normal stress in the corresponding direction while φ stands for friction angle, and c stands for cohesion of the soil.

Since the studies are conducted with non-associated flow rule, the plastic potential function is as follows:

$$g = \sqrt{J_2} + 3I_1 \sin\psi$$

where Ψ is the dilatancy angle and taken to be equal to zero for zero incompressible material definition.
Stress – Strain relationship for non-associated flow rule can be expressed as:

$$\frac{d\sigma_i^{\alpha\beta}}{dt} = \sigma_i^{\alpha\gamma}\dot{\omega}_i^{\beta\gamma} + \sigma_i^{\gamma\beta}\dot{\omega}_i^{\alpha\gamma} + 2G\dot{e}_i^{\alpha\beta} + K\dot{\varepsilon}_i^{\gamma\gamma}\delta_i^{\alpha\beta} - \dot{\lambda}_i\left[9K\sin\psi\,\delta^{\alpha\beta} + \frac{G}{\sqrt{J_2}}s_i^{\alpha\beta}\right]$$

where $\varepsilon^{\alpha\beta}$ is the strain tensor, $\dot{\lambda}_i$ is the rate of change of the plastic multiplier for the ith particle, and $\omega^{\alpha\beta}$ is the spin rate tensor values, and they are calculated for each particle i as follows:

$$\dot{\varepsilon}_i^{\alpha\beta} = \frac{1}{2}\left(\frac{\partial v_i^\alpha}{\partial x^\beta} + \frac{\partial v_i^\beta}{\partial x^\alpha}\right) = \frac{1}{2}\left[\sum_{j=1}^{N} m_j \frac{(v_j^\alpha - v_i^\alpha)}{\rho_j}\frac{\partial W_{ij}}{\partial x_i^\beta} + \sum_{j=1}^{N} m_j \frac{(v_j^\beta - v_i^\beta)}{\rho_j}\frac{\partial W_{ij}}{\partial x_i^\alpha}\right]$$

$$\dot{\omega}_i^{\alpha\beta} = \frac{1}{2}\left(\frac{\partial v_i^\alpha}{\partial x^\beta} - \frac{\partial v_i^\beta}{\partial x^\alpha}\right) = \frac{1}{2}\left[\sum_{j=1}^{N} m_j \frac{(v_j^\alpha - v_i^\alpha)}{\rho_j}\frac{\partial W_{ij}}{\partial x_i^\beta} - \sum_{j=1}^{N} m_j \frac{(v_j^\beta - v_i^\beta)}{\rho_j}\frac{\partial W_{ij}}{\partial x_i^\alpha}\right]$$

$$\dot{\lambda}_i = \frac{3\alpha_\phi K\dot{\varepsilon}_i^{\gamma\gamma} + \left(\frac{G}{\sqrt{J_2}}\right)s_i^{\alpha\beta}\dot{\varepsilon}_i^{\alpha\beta}}{27\alpha_\phi K\sin\psi + G}$$

where m_j is mass, and ρ_j is the density of the particle j while K, and G stand for Bulk Modulus, and Shear Modulus, respectively.

3 Failure Mechanism of Shallow Footing Penetration

In this section of the study, failure mechanism of a strip footing being penetrated into granular soil is observed with the use of SPH, and the findings are compared with the commercial FE software PLAXIS results, and the failure mechanism proposed by Terzaghi (1943). The material behavior is determined by the use of Drucker-Prager constitutive model with non-associated flow rules.

Strip foundation penetration into granular soil analysis has been conducted using plane strain model as shown in Figure 1. Boundaries are defined to the model by the use of ghost particles to simulate roller supports at the sides, and boundary particles to simulate pin support at the bottom (Bui et al., 2008). Moreover, the strip foundation is taken to be linearly elastic.

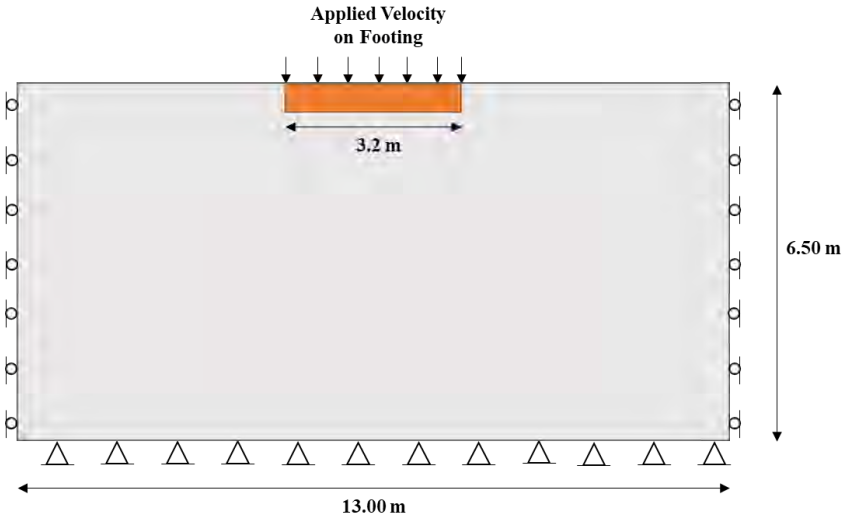

Figure 1. Numerical Model Geometry

The soil parameters are selected for 3 types that are loose, medium dense, and dense sand, and the values are tabulated below (Bowles, 1996; Marr and Hawkes, 2010; Obrzud and Truty, 2018):

Table 1. Material Properties

Type of Sand	E (MPa)	Φ (degrees)	γ (kN/m3)	ν
Loose	20	31	16	0.3
Medium Dense	40	34	18.5	0.33
Dense	65	39	19.5	0.38

where E represents Young's Modulus, Φ is the friction angle, γ is the unit weight, and ν is the Poisson's ratio of the soil.

For the SPH model, 8646 particles were used to model the soil, while 1365 particles were used to define the boundaries. The distance between the particles in both x- and y-directions is 0.1 m. The material properties of the soil particles are updated based on motion equations, while the boundary particles' properties are updated based on their types with respect to their neighbor soil particles. While applying artificial viscosity, c_a is calculated based on the following formula (Bui, 2011):

$$c_a = \sqrt{E_a / \rho_a}$$

where c_a is the wave speed, E_a is the Young's Modulus, and ρ_a is the density of particle a.

In addition to artificial viscosity application, a local damping term is proposed into the momentum equation in order to damp out the unphysical oscillations, and eliminate tensile instabilities. The soil is first set to its initial state under its own weight, then the footing particles are penetrated into soil with a constant speed of 1 cm/s.
In the FE model, same soil properties are used, and 1460 15-nodes triangular elements are used. The foundation is pushed into the ground with a constant speed of 1 cm/s.

In order to compare SPH and FE results, very loose sand parameters are defined to both models; therefore, deeper penetrations are allowed, and more results are observed. Figure 2 shows the total vertical stress at the bottom of the foundation vs depth of penetration graphs for both models:

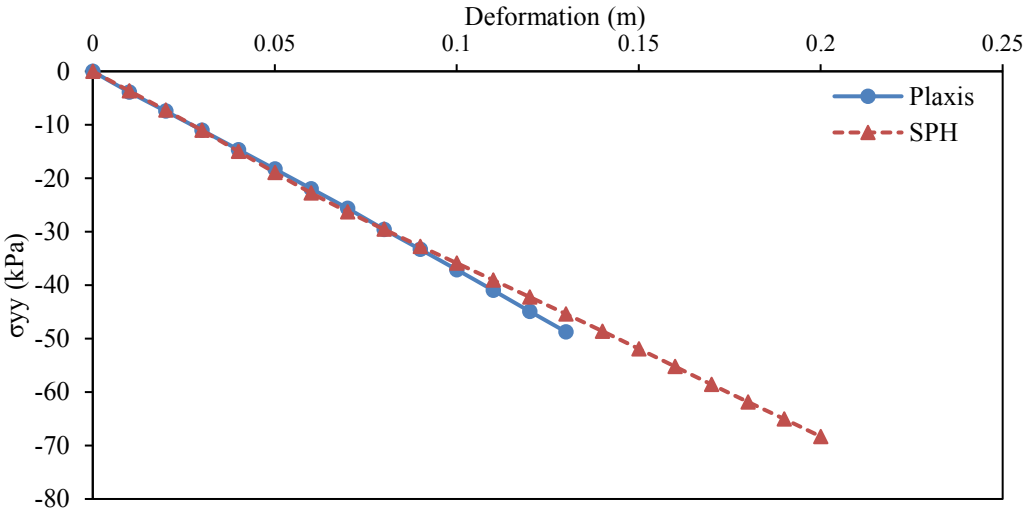

Figure 2. Stress vs Deformation for FE and SPH Methods

In Figure 2, it can be observed that at each penetration depth, the total vertical stress values are quite close to each other. Moreover, one can also observe that as the penetration proceeds, PLAXIS stops calculating results at around 13 cm while SPH goes deeper without any stability issues. The SPH model is forced to stop at 20 cm manually.

There are 3 types of failure mechanisms defined by Terzaghi (1943), and according to him, one should expect to see general failure for dense, local failure for medium dense, and punching failure for loose sand (Figure 3).

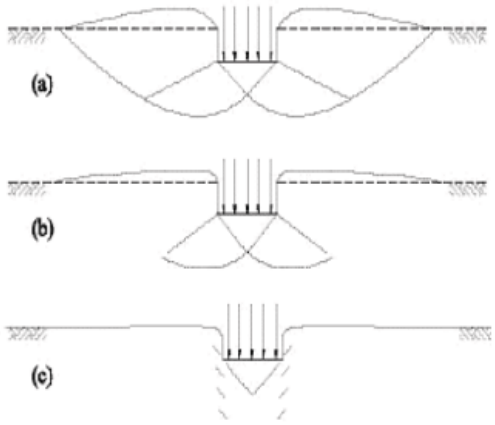

Figure 3. (a) General, (b) Local, (c) Punching Shear Failure in Foundation Soil (Terzaghi, 1943)

For a strip footing, Terzaghi's equation for the ultimate bearing capacity q_u can be expressed as follows:

$$q_u = cN_c + qN_q + \frac{1}{2}\gamma BN_\gamma$$

where c is the cohesion, q is the overburden pressure, and γ is the specific weight of the soil, and B is the width of the foundation. N_c, N_q, and N_γ are the dimensionless bearing capacity factors based on the friction angle Φ.

4 Results

As mentioned in Section 3 of this study, 3 types of granular material are used for the analysis. Figure 4 shows the loose sand results from both SPH and FE methods. It can be seen that the SPH and PLAXIS FE models predict similar stress values in y-direction, and both the failure surfaces are similar to each other. SPH shows the triangular zone right below the foundation, and there are multiple failure surfaces under that triangle. From Figure 3 (c), this type of failure can be called as a punching failure, and it is as expected for loose type of sands.

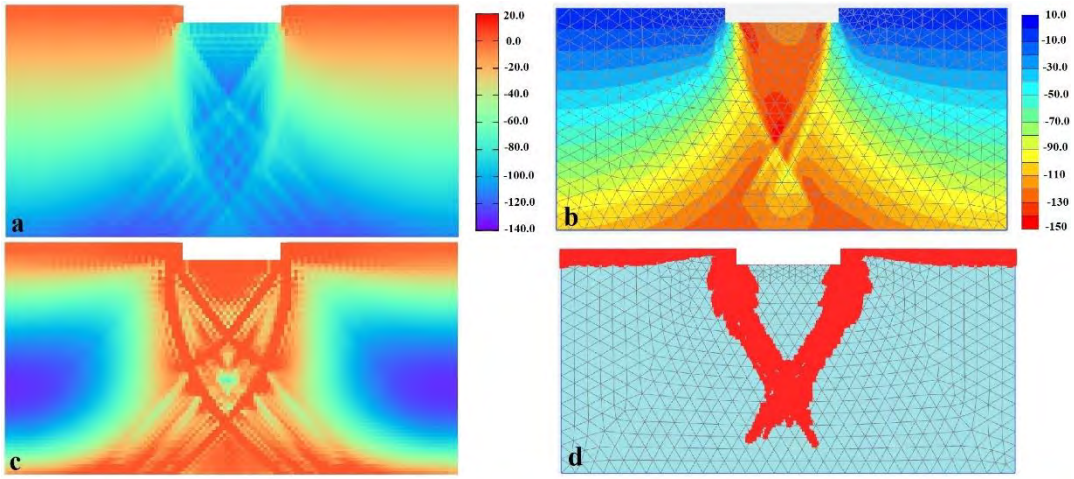

Figure 4. Loose Sand Analysis at 5 cm depth of penetration (a) SPH results for total vertical stress in kPa (b) FE results for total vertical stress in kPa (c) SPH Plastic Points (d) FE Plastic Points

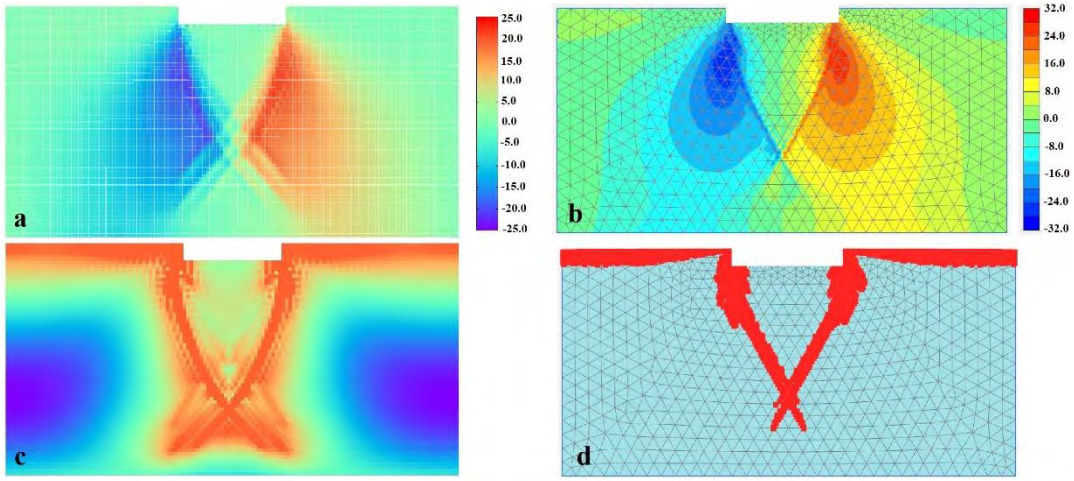

Figure 5. Medium Dense Sand Analysis at 5 cm depth of penetration (a) SPH results for total shear stress in kPa (b) FE results for total shear stress in kPa (c) SPH Plastic Points (d) FE Plastic Points

In Figure 5, footing penetration results into medium dense sand are presented. According to Figure 3(b), a local shear failure phenomena should be expected from these analyses. Figure 5(a) and 5(b) show shear stress results in SPH, and FE analyses, respectively. The shearing zones are similar to each other, and do not extend up to the ground surface, i.e., do not include Rankine Passive Zones depicting that the type of failure is a local shear failure.

Figure 6 represents the results for footing penetration into dense sand. Compared to medium dense sand results, penetration into dense type of sand gives more distinct triangular, and radial shear zones. However, as expected from general failure mechanism, the Rankine passive zone is not observed for this type of sand, either. That might be because of the use of non-associated flow rule since the dilatancy angle in this case is set to be zero in the analyses (Bui, 2011), or because the bottom boundary is not deep enough.

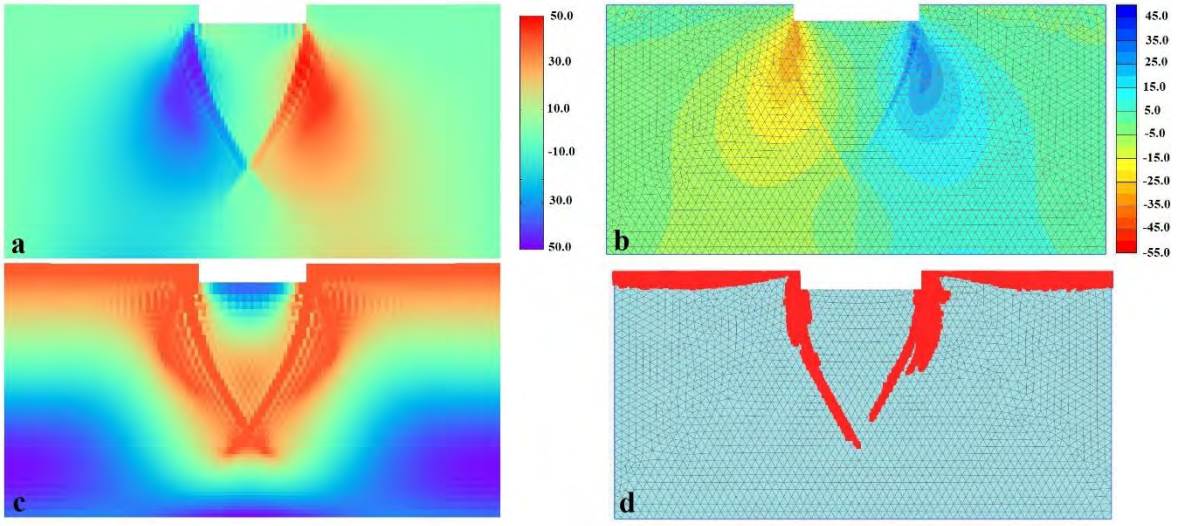

Figure 6. Dense Sand Analysis at 1 cm depth of penetration (a) SPH results for total shear stress in kPa (b) FE results for total shear stress in kPa (c) SPH Plastic Points (d) FE Plastic Points

Apart from the comparison of failure mechanisms, bearing capacities are also tabulated in Table 2. For loose, and medium dense sands, since punching, and local shear failure modes are expected, a correction to the friction angles are made based on the equation below (Birand et al., 2011), and the bearing capacity factors are selected based on the modified friction angles. The modified bearing capacity values are tabulated in the last column of the table. For loose, and medium dense sand, SPH bearing capacity results are slightly lower than the ones of FE, while both of the numerical methods are overestimating compared to modified ultimate bearing capacity formula proposed by Terzaghi (1943). For the dense sand, PLAXIS FE method could not get to the ultimate bearing capacity point, while SPH is underestimating compared to the general formula given below.

$$\phi^* = \tan^{-1}\left(\frac{2}{3}\tan\phi\right)$$

Table 2. Bearing Capacity Values (in kPa)

Type of Sand	q_f (SPH)	q_f (FE)	q_f (Terzaghi)	q_f (Terzaghi Modified)
Loose	250	264	561	124
Medium Dense	541	557	1091	487
Dense	1976	-	2298	-

5 Conclusion

This study presents the use of Smoothed Particle Hydrodynamics (SPH) Method with Drucker-Prager constitutive model with non-associated flow rule for failure mechanisms and bearing capacity of shallow foundation penetration into cohesionless soil of 3 types.

For loose and medium dense soils, there is a good agreement of results between FE and SPH methods. However, both methods seem to overestimate the bearing capacity results compared to Terzaghi's modified equation. On the other hand, for dense sand, SPH result is underestimating with respect to Terzaghi's equation, while it cannot be compared with FE PLAXIS because of the numerical errors the FE method suffers as the penetration goes on. For all types of sands analyzed in the paper, the failure mechanisms are quite similar to each other, and as expected. Punching, and local shear failures are both observed in two compared methods; however, for the dense sand, Rankine passive zone is not observed. This study shows that SPH is a powerful tool for observing failure mechanisms and calculating bearing capacity of cohesionless type of soils deforming under shallow footings.

6 References

Birand, A., Ergun, U. and Erol, O. (2011). Foundation Engineering 1, Ankara, Turkey.

Bowles, J.E. (1996). Foundation Analysis and Design. 5th Edition, The McGraw-Hill Companies, Inc., New York.

Bui, H. H. (2011). Bearing capacity bearing capacity of shallow foundation by smoothed particle hydrodynamics (SPH) analysis. *2nd International Symposium on Computational Geomechanics (COMGEO II)*.

Bui, Ha H., Fukagawa, R., Sako, K. and Ohno, S. (2008). Lagrangian meshfree particles method (SPH) for large deformation and post-failure of geomaterial using elastic-plastic soil constitutive model.

Gingold, R. A. and Monaghan, J. J. (1977). Smoothed particle hydrodynamics: theory and application to non-spherical stars, 375–389.

Lucy, L. B. (1977). A numerical approach to the testing of the fission hypothesis, 1013–1024.

Marr, W. A. and Hawkes, M. (2010). Displacement-Based Design for Deep Excavations. *2010 Earth Retention Conference (ER2010)*, 82–100.

Monaghan, J. J., & Lattanzio, J. C. (1985). A refined particle method for astrophysical problems, 135–143.

Monaghan, J. J. (1992). Smoothed particle hydrodynamics. *Annual Review of Astronomy and Astrophysics*, 543–574.

Monaghan, J. J. (2005). Smoothed particle hydrodynamics. *Reports on Progress in Physics*, 1703–1759.

Obrzud, R. F. and Truty, A. (2018). The hardening soil model - a practical guidebook.

Terzaghi, K., (1943). Theoretical Soil Mechanics, 5th ed., John Wiley & Sons Inc., New York, N.Y.